

# Mind The Edge: Refining Depth Edges in Sparsely-Supervised Monocular Depth Estimation

Lior Talker<sup>1</sup>   Aviad Cohen<sup>1</sup>   Erez Yosef<sup>1,2</sup>   Alexandra Dana<sup>1</sup>   Michael Dinerstein<sup>1</sup>

<sup>1</sup>Samsung Israel R&D Center, Tel Aviv, Israel

{lior.talker, aviad.cohen, alex.dana, m.dinerstein}@samsung.com

<sup>2</sup>Tel Aviv University, Israel

erez.yo@gmail.com

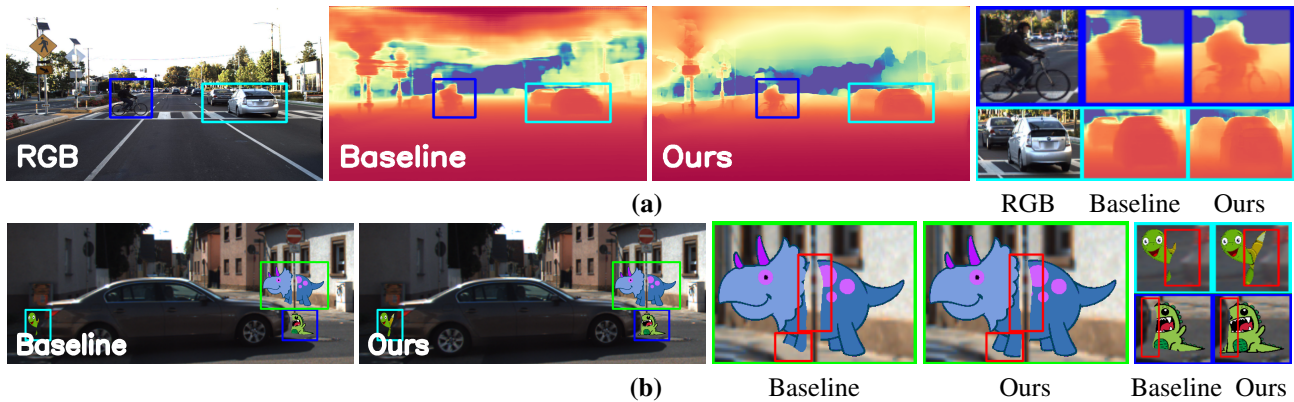


Figure 1. **Refining depth edges with our method when using Packnet-SAN [18] as an MDE baseline.** (a) Depth estimation (DDAD dataset). Zoom-in on the crops (on the right) to see the improvement in the 2D localization of the depth edges between the baseline and our method. (b) Augmented reality. An example of virtual objects planted in a scene from the KITTI dataset for AR applications. Zoom-in and inspect the boundaries for the best impression of the depth edges accuracy.

## Abstract

Monocular Depth Estimation (MDE) is a fundamental problem in computer vision with numerous applications. Recently, LIDAR-supervised methods have achieved remarkable per-pixel depth accuracy in outdoor scenes. However, significant errors are typically found in the proximity of depth discontinuities, i.e., depth edges, which often hinder the performance of depth-dependent applications that are sensitive to such inaccuracies, e.g., novel view synthesis and augmented reality. Since direct supervision for the location of depth edges is typically unavailable in sparse LIDAR-based scenes, encouraging the MDE model to produce correct depth edges is not straightforward. In this work we propose to learn to detect the location of depth edges from densely-supervised synthetic data, and use it to generate supervision for the depth edges in the MDE training. To quantitatively evaluate our approach, and due to the lack of depth edges ground truth in LIDAR-based scenes, we manually annotated subsets of the KITTI and the DDAD datasets with depth edges ground truth. We demonstrate significant gains in the accuracy of the depth edges with

comparable per-pixel depth accuracy on several challenging datasets.

## 1. Introduction

Monocular Depth Estimation (MDE) aims to recover the depth of each pixel in a single RGB image. It is used in many important applications, such as robotic navigation [11], novel view synthesis [7] and Augmented Reality (AR) [33]. Nonetheless, MDE is an ill-posed problem; that is, a single RGB image may be generated from many possible scenes. However, in recent years, many MDE methods, based on Convolutional Neural Networks (CNNs) have shown remarkable results. CNN-based supervised methods are trained with depth Ground Truth (GT) which is usually dense for indoor scenes, e.g., acquired using a RGBD camera [47], and sparse for outdoor scenes, e.g., acquired using a LIDAR sensor [15].

It was observed in several papers [35, 58, 65] that the 2D locations of depth discontinuities, which we refer to as *depth edges* in this paper, are often poorly estimated, resulting in thick smooth depth gradients or incorrectly-localized

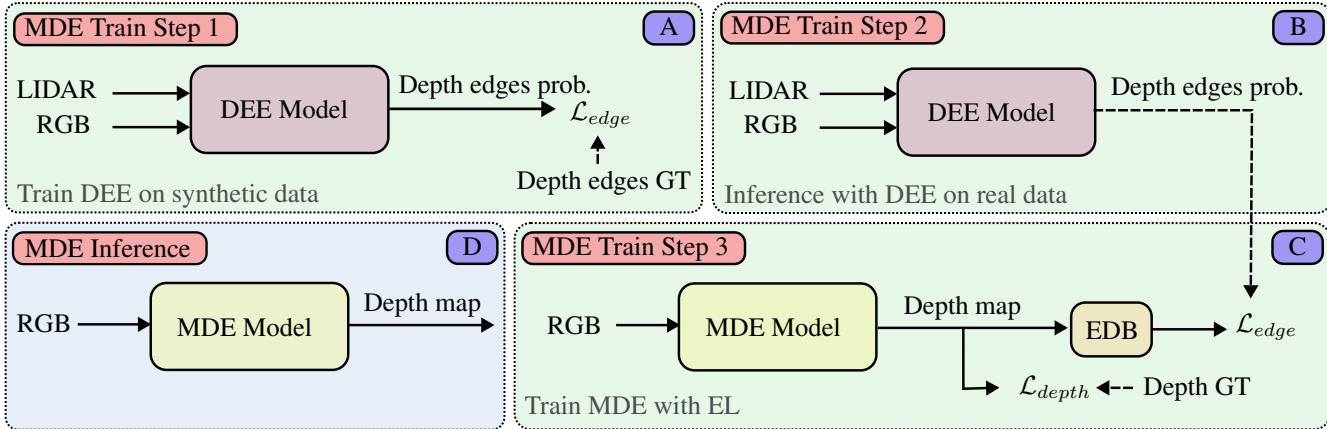


Figure 2. **Overview of our proposed MDE training method.** (A) Training the DEE model on synthetic data. (B) Inferring depth edges on the training set of the real data using the trained DEE model. (C) Training the MDE model on real data with the Edge Loss (EL) using the supervision from the previous step. (D) Inference using the MDE model on the real data. Solid and broken lines represent the dataflow and the GT used in loss functions, respectively.

edges (see the baseline in Fig. 1). Some applications that use predicted depth maps are highly sensitive to errors in depth edges, which are often part of the silhouette of objects. One example of such an application is Novel View Synthesis (NVS) – generating a new view of a scene captured from one or more views. In NVS methods that use depth explicitly [7], these type of localization errors in the 2D location of depth edges, may result in wrongly localized object parts in another newly generated view. Another important application that often uses predicted depth is virtual object rendering for AR [33], which computes for each pixel the closest occluding object from the point of view of the user. When relying on inaccurate depth edges in the computation of the occlusion, significant artifacts and unrealistic appearance may occur (see Fig. 1).

The underlying reasons for the difficulty in properly reconstructing depth edges are probably twofold. The first is the small impact of the depth edges on the network’s loss since they occupy only a tiny portion of the image. The second, which is partially discussed in [10, 60], is due to alignment errors between the RGB image and the LIDAR signal. Specifically, LIDAR measurements are often wrongly associated with objects although belonging to the background, or absent in occluded areas that are revealed in the time gap between the RGB and the LIDAR data acquisition (Fig. 3b). This phenomenon is also depicted in Fig. 3a for the raw LIDAR of the KITTI dataset [15], where regions close to depth edges suffer from a lower density of LIDAR measurements.

In this paper we propose to improve the accuracy of the depth edges in MDE methods by directly encouraging the depth edges of the predicted depth map to be well-localized. Assuming that depth edges GT is available, a dedicated *depth edges loss* that encourages the network to generate

sharp discontinuities in the correct locations may be used. However, due to the sparsity of the depth GT in typical outdoor scenes (e.g., KITTI), which are considered in this paper as our target domain, obtaining accurate depth edges GT is a challenging task.

To this end, we propose to train a Depth Edge Estimation (DEE) network (Sec. 3.5), which predicts the probability that a pixel is located on a depth edge, using an accurate dense depth GT of a synthetic dataset, the GTA-PreSIL [25] (Fig. 2A). Using the DEE network we infer a probabilistic map of depth edges on the training set of the target real domain (Fig. 2B). These maps are then used to guide the proposed edge loss in the training of the MDE network (Fig. 2C). Although training on synthetic data and inferring on real data is notoriously known to lead to poor performance due to a large ‘domain gap’ [37, 43], our experiments (Sec. 4) demonstrate that the DEE network performs well in practice.

Due to the lack of depth edges GT for evaluation in LIDAR-supervised real-world datasets, we manually annotated depth edges in two evaluation sets of 115 and 50 images from the KITTI and DDAD datasets, respectively (see an example in the top of Fig. 6). We show on these newly annotated datasets that our approach generates depth with significantly more accurate depth edges than the MDE baseline, while maintaining a similar depth accuracy. These datasets will be made publicly available upon publication.

Our main contributions are twofold:

- A novel method to improve the localization of depth edges in MDE methods while preserving their per-pixel depth accuracy.
- A benchmark of annotated depth edges to evaluate their quality in sparsely-supervised MDE algorithms.

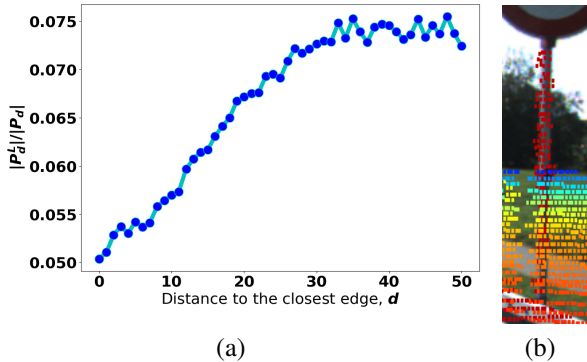


Figure 3. **The density of the LIDAR near edges in a partial set of the KITTI dataset (our proposed KITTI-DE dataset).** Denote the set of all pixels with a distance  $d$  to the closest edge as  $P_d$ , and the set of pixels,  $p$ , in  $p \in P_d$  with LIDAR measurement as  $P_d^L$ . (a) The ratio of LIDAR measurements,  $|P_d^L|/|P_d|$ , out of all pixels in  $P_d$ , as a function of  $d$ . (b) An example from the KITTI dataset of a gap in the LIDAR measurements (left of the pole) and an infiltration of LIDAR measurements from the background to the pole (right of the pole). For visualization purposes the LIDAR measurements are dilated.

## 2. Previous Work

Depth estimators can be trained using full supervision with LiDAR or other absolute depth measurements [3, 4, 18, 26, 28, 31, 48, 50], by self-supervision using two or more RGB images [8, 16, 17, 19, 21–23, 32, 36, 46, 52, 55, 64] or using semi-supervision [2, 24, 30, 56]. The main objective of these methods is to reduce the overall mean absolute relative error (ARE), recently achieving state-of-the-art (SOTA) result with ARE close to 5% on the KITTI dataset [4, 18]. However, specific applications such as AR require that the edges of the predicted depth are also accurate.

To achieve this, various depth estimation models were trained in a fully-supervised manner using dense depth GT. Such datasets include the indoor large-scale NYU-2 dataset [47] that was collected with the low-range Microsoft-Kinect and the small scale but highly accurate IBims-1 [29] and Middlebury [44] datasets. Dense outdoor depth maps include the small scale ETH3D [45] dataset and large-scale DIODE [53]. SharpNet [39] improved depth prediction on object edges in indoor scenes by predicting occluding contours. Their solution was first pretrained to predict occluding contours on synthetic data and then fine-tuned on the indoor NYUv2 dataset to constrain normal, depth and occluding contours. In its subsequent work [38] the authors predicted displacement fields of pixels with poorly predicted depth values of dense depth maps. DCTNet [63] boosted the resolution of depth maps from low-resolution ones using an edge attention mechanism and high-resolution RGB images. In their work the authors assume co-occurrence be-

tween the texture edges of RGB images and depth edges. However, their method is also fully-supervised trained on dense depth maps such as NYUv2 [47] and Middlebury [44]. These methods require training on dense GT depth maps collected using expensive short-range laser scanners which are mostly ineffective for outdoor scenes.

A family of recent works used synthetic data, in particular the VirtualKITTI dataset [5, 13] during training to improve depth resolution [9, 24, 49, 61, 62]. The advantage of the VirtualKITTI dataset is its structural similarity to the target KITTI dataset. Nonetheless, these works achieved an ARE higher than 10%. In our work we demonstrate how we overcome a more significant domain gap between the used synthetic data and our target domains with a significantly lower ARE.

Other works utilized the partial consistency between the edges between semantic classes in semantic segmentation maps and depth edges to improve the depth predictions on these regions. A dedicated loss was developed [65] which slightly improved the ARE near the edges of the segmentation masks. Another work [42] used stereo images and panoptic segmentation maps during training to refine depth edges, achieving an ARE of 10.3% on the KITTI dataset. SGR [58] also used semantic segmentation and pseudo-GT depth maps created from disparity maps to improve depth predictions near depth edges using a dedicated loss. Although achieving impressive visual results, SGR achieved an ARE of 17.9% on the KITTI dataset. Contrary to these approaches, in this work we improve depth edges without using additional segmentation maps from the target domain, while achieving comparable ARE to SOTA solutions.

In an attempt to overcome the sparsity limitation of ground-truth depth maps for outdoor scenes, disparity maps were generated from the 3D Movies Dataset [41] using publicly available stereoscopic movies from various scene types. However, stereo matching is a non-trivial task and the quality of the maps claimed to be 'medium'. Moreover, without knowing the exact baseline and other camera characteristics, the estimated depth maps units cannot be metric-reconstructed as needed for automotive solutions requiring absolute depth estimations. MiDAS [41] and DPT [40] models were also trained on this dataset, achieving visually striking depth maps. However, the lack of absolute scale of the training data limits these models from predicting absolute depth values.

In a recent work, Miangoleh et al. [35] introduced a method that blends the original predicted depth map with depth maps of the source image at different resolutions. The accuracy of this method was evaluated using order ranking around depth edges, but did not measure the absolute depth metrics on automotive related datasets, such as the KITTI dataset. We compare between this method, which we call BoostingDepth, and our method in Sec. 4.5 and show its

limitations for automotive applications.

### 3. Method

The flow of our MDE training method can be described in three steps as illustrated in Fig. 2A-C. In the first step, the DEE network is trained on the source synthetic dataset with the depth edges GT, to predict a probabilistic map of depth edges for a given RGB image and the corresponding LIDAR measurement (Fig. 2A and Sec. 3.5). In the second step, inference is applied on the training set of the target real data using the trained DEE network, resulting in (approximate) depth edge labels,  $\tilde{E}_{GT}$  (Fig. 2B). In the last step we train the MDE network with an Edge Detection Block (EDB) to improve the localization of the depth edges (Fig. 2C and Sec. 3.2). The training is carried out using a straightforward supervised depth loss with LIDAR as GT, and the proposed edge loss with  $\tilde{E}_{GT}$  as approximate GT. In the following sections we describe our method and the used steps in detail.

#### 3.1. Monocular Depth Estimation

MDE models are commonly trained to regress per-pixel depth,  $D(I)$ , from an RGB image,  $I$ , given a depth GT,  $D_{GT}$ , in  $S$  scales, using a loss function:

$$\mathcal{L}_{depth}^{ms} = \frac{1}{S} \sum_s \mathcal{L}_{depth}(D^s(I), D_{GT}^s), \quad (1)$$

where  $D^s(I)$  and  $D_{GT}^s$  indicate the predicted depth and GT depth in scale  $s$ , respectively. For brevity we omit the scale indexes for the rest of the paper, although, unless explicitly stated, all losses are multi-scale.

#### 3.2. Edge Detection Block (EDB)

To encourage the model to produce sharp edges at the correct locations, we use a differentiable layer that computes the per-pixel probability of depth edges,  $\tilde{E}(D(I))$ , from the predicted depth map,  $D(I)$ , where  $I$  is the input RGB image. Given  $D(I)$ , the EDB computes the magnitude of the spatial image gradient,  $|\nabla D(I)|$ , and then transforms it into an 'edge-ness' probability score:

$$\tilde{E}(D(I)) = \text{sigmoid}(|\nabla D(I)| - t_{grad}) \quad (2)$$

by thresholding it with the parameter  $t_{grad}$  and passing it through a sigmoid function.

In practice, when using the standard image gradient

$$|\nabla D(I)| = \sqrt{\left(\frac{dD(I)}{dx}\right)^2 + \left(\frac{dD(I)}{dy}\right)^2},$$

some cyclic gradient patterns may emerge since both  $dD(I)/dx$  and  $dD(I)/dy$  are unconstrained (see depiction in the supplementary material). Therefore, we compute the

gradient as a derivative in the direction perpendicular to the edge. To this end, the normal direction to the edge is first computed from the depth edge GT,  $\tilde{E}_{GT}$ , by:

$$\theta = \text{atan2}\left(\frac{d\tilde{E}_{GT}}{dy}, \frac{d\tilde{E}_{GT}}{dx}\right)$$

The derivative in the direction perpendicular to the edge for every pixel  $(x, y)$  is therefore given by:

$$\nabla_{\theta} D(I(x, y)) = D(I(x + \cos \theta, y + \sin \theta)) - D(I(x - \cos \theta, y - \sin \theta))$$

where the coordinates  $x \pm \cos \theta$  and  $y \pm \sin \theta$  are rounded in practice. The predicted edge probability,  $\tilde{E}(D(I))$ , is then used by the depth edges loss as described in the following section.

#### 3.3. Depth Edges Loss

Given the depth edges GT,  $\tilde{E}_{GT}$ , and the output of the EDB,  $\tilde{E}(D(I))$ , we use the following loss to encourage sharp edges at  $\tilde{E}_{GT}$ :

$$\mathcal{L}_{edge}(\tilde{E}(D(I)), \tilde{E}_{GT}) = BBCE(\tilde{E}(D(I)), \tilde{E}_{GT}) \quad (3)$$

where the *BBCE* [59] is the Balanced Binary Cross Entropy loss where the positives (edge pixels) and the negatives (non-edge pixels) are reweighted in a standard BCE loss so they have equal contribution.

#### 3.4. Total Loss

Our MDE model is trained with a linear combination of the edge loss,  $\mathcal{L}_{edge}$ , and the standard depth loss,  $\mathcal{L}_{depth}^{ms}$  (Eq. 1). The total loss is given by

$$\mathcal{L} = \mathcal{L}_{depth}^{ms}(D(I), D_{GT}) + \alpha \mathcal{L}_{edge}(\tilde{E}(D(I)), \tilde{E}_{GT}), \quad (4)$$

where  $\alpha$  is a parameter to balance between the two losses, and  $D_{GT}$  is the depth GT.

#### 3.5. Depth Edges Estimation (DEE)

Since the actual depth edges GT is unavailable for the target real data we use the DEE network, which predicts depth edges,  $\tilde{E}(I, D')$ , from RGB,  $I$ , and LIDAR,  $D'$ . We note that the LIDAR measurements have significant impact on the performance of the DEE network when given as input in addition to the RGB (ablation study is presented in the supplementary material). In order to train the DEE network we use a synthetic dataset with dense depth and LIDAR that are available for each RGB image. To extract depth edges GT,  $E_{GT}$ , we use the Canny edge detector [6] on the dense depth GT. The DEE network is trained with the depth edges loss as presented in Eq. 3; that is,  $\mathcal{L}_{edge}(\tilde{E}(I, D'), E_{GT})$ .

The predicted depth edges,  $\tilde{E}(I, D')$ , obtained from the DEE network are dense with Gaussian-like distributions. To produce sharp edges that are one pixel wide, we use two standard post-processing operations from the edge detection literature [6]: (a) Non-Maximum Suppression (NMS), and (b) hysteresis (with 0.85 and 0.9 as low and high parameters, respectively).

## 4. Experiments

In the following sections we describe various experiments that demonstrate the effectiveness of our suggested method and compare it to the SOTA and other relevant methods.

### 4.1. Implementation Details

The DEE network follows the architecture of the U-net like PackNet-SAN [18] which was used as an MDE network. One of the beneficial properties of PackNet-SAN is its sparse encoder for the sparse LIDAR signal, which uses only sparse layers (e.g., sparse convolutions), which is suitable for our case of depth edges estimation. The DEE network is trained for five epochs on the GTA-PreSIL dataset [25], which is presented in the next section.

### 4.2. Datasets

The GTA-PreSIL dataset is rendered from the Grand Theft Auto (GTA) video game. It consists of  $\sim 44$ K images for training and  $\sim 7$ K images for validation and testing, where each image has a corresponding dense depth GT. To generate the GT for the depth edges, we use Canny edge detector [6] with low and high thresholds of 4 and 5 meters, respectively. We note that the DEE network could have been trained with Virtual KITTI [13], probably achieving better performance on KITTI (details below) due to a smaller domain gap between the datasets. However, since we aim to demonstrate a general-purpose DEE network, GTA-PreSIL was the better choice since its structures and styles are significantly different from the target real domains.

We demonstrate our method on three different datasets: Synscapes [57], KITTI [51] and DDAD [20]. The data split for the highly realistic synthetic dataset Synscapes is 20K, 1K and 4K images for training, validation and test, respectively, as described in [54]. Each image has a corresponding dense depth, semantic and instance segmentation. It is also interesting to note that almost all images in Synscapes are crowded with cars and pedestrians, which is significantly different than common datasets, such as KITTI and DDAD. We have chosen this dataset since it (1) provides free and perfect depth edges GT to evaluate our method, and (2) it has dense depth that allows us to fully analyze the impact of our method on the per-pixel depth accuracy in comparison to the baseline.

For the KITTI dataset we use the Eigen split [12] which consists of  $\sim 40$ K training images and 697 testing images. For the DDAD dataset we use the official split with  $\sim 12$ K images for training and  $\sim 1200$  images for validation. Importantly, it is not clear how to evaluate the depth edges quality of an MDE network on both the KITTI and the DDAD datasets since they have only sparse LIDAR.

**KITTI & DDAD Depth Edges Evaluation Sets:** To enable direct evaluation of the depth edges of MDE networks on the KITTI and DDAD datasets, we introduce the KITTI Depth Edges (KITTI-DE) and the DDAD Depth Edges (DDAD-DE) evaluation sets which consist of depth edges annotations of 115 images from the KITTI dataset and 50 images from DDAD dataset, respectively. To ease the manual annotation process, we started from the 115 images of the Semantic and Instance Segmentation evaluation benchmark of KITTI [1] and 50 images of the validation set of DDAD. To get an initial approximation of the depth edges we derive the edges of the instance segmentation masks for the relevant classes, and the semantic segmentation maps for the other classes. Then, false depth edges were manually removed (e.g. car wheels point of contact on the road), and missing depth edges were added (e.g., edges between building). The KITTI-DE and DDAD-DE evaluation sets will be published upon acceptance.

### 4.3. Metrics

To evaluate the performance of the MDE networks, we use some of the common MDE (per-pixel) depth metrics, as well as metrics to evaluate the quality of the edges of the predicted depth. Both depth and depth edges are evaluated in the bottom 60% of the image where LiDAR is commonly available, as defined in Garg et al. [14], for all datasets.

**Depth metrics:** We use the common Absolute Relative Error (ARE) to measure the per-pixel regression depth error, which is given by  $ARE(\tilde{d}, d) = |\tilde{d} - d|/d$ , where  $\tilde{d}$  and  $d$  are the predicted depth and GT depth, respectively. Note that the ARE is computed only over the sparse LIDAR measurements in the KITTI and the DDAD datasets, which are very sparse near edges (Fig. 3), making the ARE a poor metric to measure the quality of the 2D localization of depth edges.

**Depth edges metrics:** To evaluate the edge quality of the predicted depth, one option that was recently used is the ORD metric [58]. The ORD metric measures the percentage of order disagreements between pairs of depth points in the predicted depth against the GT depth. We argue that this metric suffers from a similar problem as the ARE - since LIDAR measurements are sparse, many possible 2D edges can obtain the same ORD value.

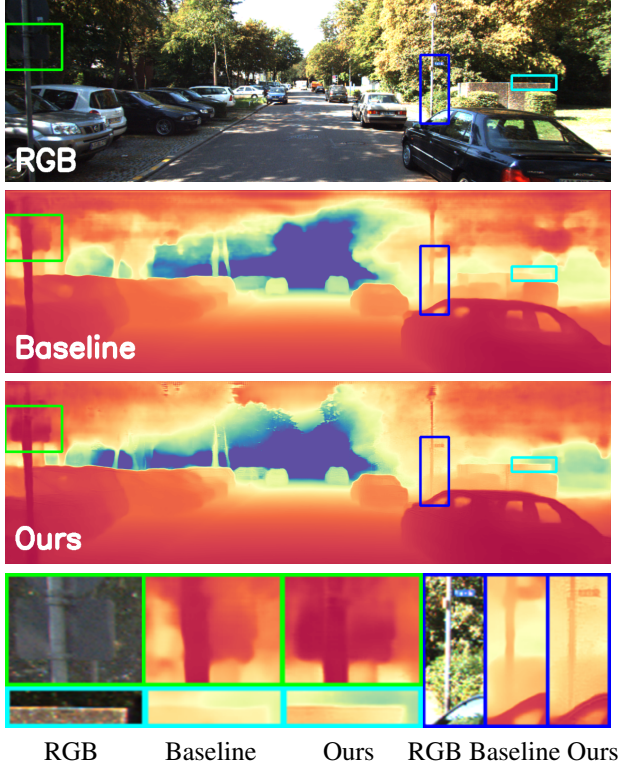


Figure 4. **Examples of depth predictions in the KITTI-DE dataset.** The depth predictions for the baseline and our method correspond to Packnet-SAN and Packnet-SAN+EL, respectively.

Therefore, in addition to the ORD metric, we use the most common metric from the edge detection literature, BSDS [34]. It consists of finding a bijective matching,  $\mu(\tilde{E}, E)$ , between the edge pixels of the predicted depth,  $\tilde{E}$ , and the edge pixels of the GT,  $E$ . Each match  $(\tilde{e}, e) \in \mu(\tilde{E}, E)$  between edge pixel,  $\tilde{e} \in \tilde{E}$ , and edge pixel GT,  $e \in E$ , is obtained such that the locations of the pixels are similar; that is,  $\|\tilde{e}, e\|_2 \leq t_e$  where  $t_e$  is a small threshold (we use  $t_e = 2$ ). The precision,  $PR(\tilde{E}, E)$ , and recall,  $RE(\tilde{E}, E)$ , are then given by  $|\mu(\tilde{E}, E)|/|\tilde{E}|$ , and  $|\mu(\tilde{E}, E)|/|E|$ , respectively.

In practice,  $\tilde{E}$  is obtained by extracting edges from the predicted depth  $d$  using Canny edge detector with low and high thresholds of  $th_{low}$  and  $th_{high}$ , respectively. Since there is an inherent tradeoff between the precision and recall, we invoke multiple runs of a Canny edge detector with different parameters to obtain a precision-recall curve. Finally, to quantify the depth edges quality in a single number, we compute the Area Under the Curve (AUC). Since a large part of the graph is uncovered by all MDE algorithms, we report both the AUC for a partial representative range and for all range  $([0,1])$ .

## 4.4. Results

We use our method with two SOTA sparsely-supervised MDE methods as baselines: Packnet-SAN [18] and AdaBins [4]. For both methods we use the publicly available code and weights and resume training for ten more epochs with our proposed loss (Sec. 3.3), and without it as a baseline for the comparison. We use  $\alpha = 0.1$  and  $\alpha = 1.0$  for Packnet-SAN and AdaBins, respectively. Also, we note that AdaBins is trained only with the largest scale for both baseline and our method as in the original training. In the following sections, we refer to the original methods by Packnet-SAN and AdaBins, and refer to these methods with the addition of our edge loss (Sec. 3) as Packnet-SAN + EL (ours) and AdaBins + EL (ours), where EL is abbreviation for 'Edge Loss'.

### 4.4.1 The KITTI dataset

In Fig. 4 we present an image from the KITTI-DE dataset alongside the depth predictions of the baselines and our method. It can be seen, for example on the crops in the bottom row, that our method has considerably more accurate depth edges than the baseline in many parts of the scene.

The precision-recall curves for the KITTI-DE dataset, which are presented in the leftside of Fig. 5, are computed for the baselines and competing methods (solid curves) and for our method with the edge loss (broken curves). The precision-recall curves of our method in comparison to the corresponding baselines, when compared using the same precision (same  $x$  coordinate), has significantly higher recall. In Tab. 1, the AUC metric for the edge quality is presented, where our method achieves an AUC of 62.2% and 53.47% in comparison to the Packnet-SAN and AdaBins baselines that achieve an AUC of 47.8% and 41.23%, respectively, indicating  $\sim 30\%$  of relative improvement.

The quality of the per-pixel depth is also evaluated on the KITTI-DE dataset, and the ARE is presented in Tab. 1. The Packnet-SAN and the AdaBins baselines achieve an ARE of 3.45% and 3.13%, respectively, in comparison to our Packnet-SAN + EL and AdaBins + EL that achieve an ARE of 3.61% and 3.11%, respectively, which indicates a comparable performance. We also evaluate the methods on the standard KITTI test set (Tab. 1), where only the per-pixel depth quality can be estimated. The Packnet-SAN and the AdaBins baselines achieve an ARE of 6.17% and 6.28%, respectively, in comparison to our Packnet-SAN + EL and AdaBins + EL that achieve an ARE of 6.50% and 6.21, respectively, which also indicates a comparable performance.

### 4.4.2 The DDAD dataset

In Fig. 6 we present an image from the DDAD-DE dataset, alongside the depth predictions of Packnet-SAN and our

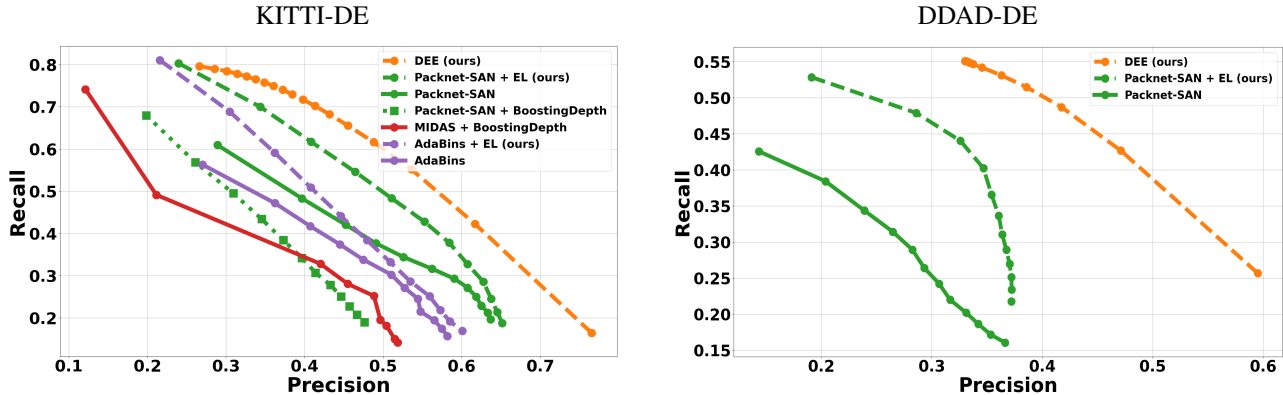


Figure 5. Precision and recall of the depth edges on the KITTI-DE and DDAD-DE evaluation sets. Each of the points on the graphs that correspond to an MDE method is generated with different parameters of the Canny edge detector. Each of the points on the graphs that correspond to the DEE method is generated by thresholding the depth edge probability in the range (0, 1).

Method	KITTI-DE				KITTI test		
	AUC (edges) $\uparrow$	ORD $\downarrow$	ARE $\downarrow$	$\delta < 1.25$ $\uparrow$	ORD $\downarrow$	ARE $\downarrow$	$\delta < 1.25$ $\uparrow$
Packnet-SAN	47.56% (39.40%)	7.68%	3.45%	98.66%	12.40%	6.17%	95.39%
Packnet-SAN + EL (ours)	<b>61.87% (49.02%)</b>	7.75%	3.61%	98.53%	12.48%	6.50%	95.06%
Packnet-SAN + BoostingDepth [35]	39.89% (35.94%)	10.14%	12.68%	85.63%	12.42%	17.58%	79.29%
MIDAS + BoostingDepth [35]	35.63% (32.75%)	13.82%	17.7%	73.83%	15.43%	17.95%	75.62%
AdaBins	41.23% (34.11%)	7.69%	3.14%	98.78%	10.14%	6.28%	95.85%
AdaBins + EL (ours)	<b>53.47% (44.00%)</b>	7.64%	3.11%	98.79%	10.13%	6.21%	95.87%

Table 1. Results on the KITTI dataset. The AUC is given for the range where at least one MDE method has valid measurement: [0.12,0.65]. In parentheses we also report the AUC of the full [0,1] range.

method with Packnet-SAN as baseline. Furthermore, the depth edges (extracted similarly to KITTI), which are laid on top of the RGB images, are presented in the top row. It can be seen that our method has considerably more accurate edges that fit more tightly on objects’ silhouette in comparison to the baseline, similarly to the KITTI dataset. It can be seen that our method has considerably more accurate edges that fit more tightly on objects’ silhouette in comparison to the baseline. Moreover, some missing edges are added and some clear false positives are discarded in our method in comparison to the baseline. Finally, we would like to note that even though our method produces accurate depth edges on the horizon line (or on the canopy of trees), the depth values are usually arbitrary (as in the baselines) since no LIDAR supervision is available there.

The precision-recall curves for the DDAD-DE dataset are presented in the right side of Fig. 5, where our method, when compared with the same precision (same  $x$  coordinate), has significantly higher recall than the Packnet-SAN baseline. In Tab. 2, the AUC metric for the edge quality is presented, where our method achieves an AUC of 48.51%

in comparison to Packnet-SAN that achieves an AUC of 31.98%, indicating around 50% of relative improvement.

The quality of the per-pixel depth is also evaluated on the DDAD-DE dataset, and the ARE is presented in Table 2. The Packnet-SAN baseline and our methods achieve an ARE of 8.89% and 8.99%, respectively, which indicates a comparable performance. On the standard DDAD evaluation set (Table 2), where only the per-pixel depth quality can be estimated. The ARE of the Packnet-SAN and our method are 9.49% and 10.0%, respectively, indicating, a 5% decrease in per-pixel depth accuracy of our method.

#### 4.4.3 The Synscapes dataset

We present the results of an additional experiment on the Synscapes dataset in Tab. 3 and in the supplementary material. In this experiment we show that an increase in the depth edges accuracy yields an increase in the per-pixel depth accuracy (e.g., ARE) for dense depth GT. It further suggests that the slight decrease in the per-pixel depth accuracy, which is sometimes observed in KITTI and DDAD, might be due to the sparseness of their depth GT, especially

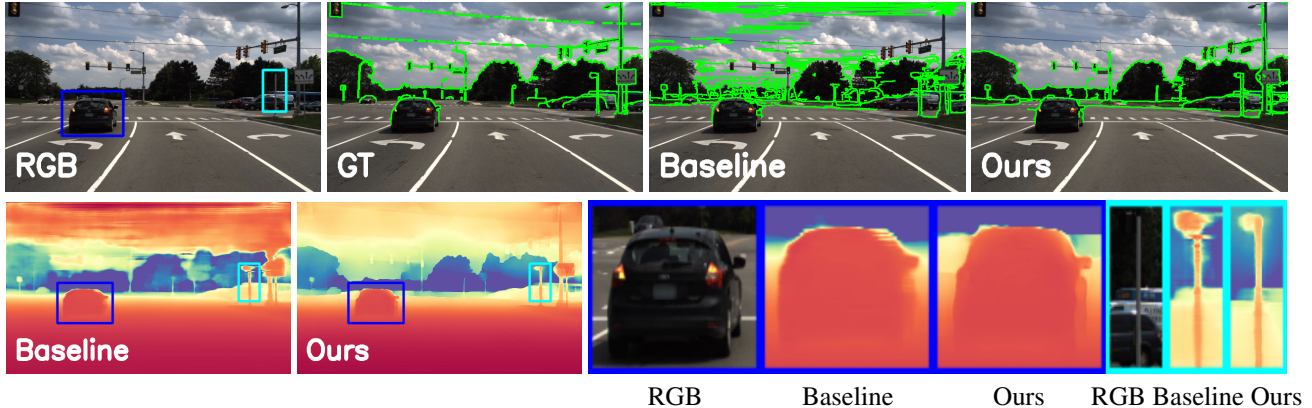


Figure 6. **Examples of depth predictions of Packnet-SAN and Packnet-SAN + EL (ours) with and image from the DDAD-DE dataset.** The top row, from left to right: RGB, depth edges GT (manually annotated), depth edges extracted using Canny edge detector from the baseline predicted depth and ours depth, respectively. The bottom row, from left to right: the predicted depth of the baseline and our method, respectively, followed by two zoom-in crops with the RGB, baseline and our predicted depth, respectively.

Method	DDAD-DE				DDAD test		
	AUC (edges) $\uparrow$	ORD $\downarrow$	ARE $\downarrow$	$\delta < 1.25$ $\uparrow$	ORD $\downarrow$	ARE $\downarrow$	$\delta < 1.25$ $\uparrow$
Packnet-SAN	31.98% (23.32%)	8.03%	8.89%	91.62%	8.95%	9.49%	90.7%
Packnet-SAN + EL (ours)	<b>48.51% (32.29%)</b>	8.38%	8.99%	91.44%	9.43%	10.0%	89.5%

Table 2. **Results on the DDAD dataset.** The AUC is given for the range where at least one MDE method has valid measurement: [0.14,0.37]. In parentheses we also report the AUC of the full [0,1] range.

Method	AUC $\uparrow$	ORD $\downarrow$	ARE $\downarrow$	$\delta < 1.25$ $\uparrow$
Packnet-SAN	61.17%	30.79%	5.43%	96.21%
Packnet-SAN + EL (ours)	<b>65.38%</b>	21.14%	4.85%	96.55%

Table 3. **Results on the Synscapes dataset.**

near depth edges.

#### 4.5. Comparison to BoostingDepth

To the best of our knowledge there are no other methods that improve the depth edges of sparsely-supervised MDE methods; however, BoostingDepth by Miangoleh et al. [35] share a similar aim to ours, even though it was designed for densely-supervised MDE methods. To this end, we use the predictions of Packnet-SAN with their depth merger for comparison with our method. The AUC and ARE metrics presented in Tab. 1 and Fig. 5 show a significantly worse performance than our method and the Packnet-SAN baseline. The reason for such performance is probably the merge network which was trained on dense indoor data. Importantly, note that BoostingDepth uses the GAN-based pix2pix framework [27] as its depth merger network. Therefore, it is not clear how to train it on sparse data since the discriminator will have to process both dense predic-

tions and sparse GT data. Visual results are presented in the supplementary material.

#### 4.6. Application: AR occlusions

To demonstrate the usability of our method, we present a simple experiment in rendering virtual objects for AR applications. We use the predicted depth of the Packnet-SAN baseline and our method to compute the occluded parts of the virtual objects from the point of view of the camera. In Fig. 1b three animated characters are planted in the scene. To observe the difference in the depth edges accuracy, zoom-in on the sides of the vehicle and on the 'no-entry' post. The occlusions of the character in our method seems much more realistic than the baseline.

### 5. Discussion

We have presented a method to improve the localization of the depth edges in the predictions of sparsely-supervised MDE methods, while preserving the per-pixel depth accuracy. The method is based on the observation that detecting the location of the depth edges can be learned effectively from synthetic data. To evaluate our method on real data, we introduced two depth edges evaluation sets for the KITTI and the DDAD datasets by manual annotation. We aspire that these evaluation sets will become standard benchmarks

to be used by the MDE community to evaluate the depth edges in addition to the standard per-pixel depth evaluation.

The proposed method can be further improved by considering the images (and LIDAR) of the target dataset (e.g., KITTI) in the training procedure, possibly using methods from the unsupervised domain adaptation literature. In addition, we believe that non-pixelwise losses (instead of the BBCE loss) can further improve the accuracy of the depth edges.

## 6. Supplementary Material

In the following section we provide additional details, examples and results for the experiments described in the main paper.

### 6.1. The Synscapes dataset

To simulate a real outdoor dataset with LIDAR supervision, we sample pixels from the dense depth GT in a typical LIDAR pattern, similarly to the KITTI dataset, with 64 vertical beams and an horizontal beam density of 0.09 degrees between beams. Since this is a naïve approach we follow the LIDAR density, presented in Fig. 3 of the main paper, and randomly remove LIDAR samples such that the resulting distribution is similar to KITTI’s. Note, however, that the true LIDAR spatial distribution in KITTI is more complex than our simulation since large continuous areas lack LIDAR samples in KITTI, in contrast to our simulation. We hypothesize that a more realistic simulation would result in worse depth edges of the baseline, increasing the depth edges performance gap from our method.

In Fig. 14 we present two images from the Synscapes dataset alongside the depth prediction of the baseline and our method (with Packnet-SAN). It can be seen that although the Packnet-SAN baseline is has mostly accurate edges, our method still outperforms it in some parts of the image. The quantitative results are presented in the main paper (Tab. 3) and in the bottom of Fig. 7, which demonstrate a small, but consistent improvement in the depth edges quality. Importantly, as argued in the main paper, the per-pixel metrics, e.g., ARE, of our method is significantly better, which suggests that when dense depth is available, the improvement in the edge quality is translated into an improvement in the per-pixel depth metrics.

### 6.2. Additional Examples for KITTI and DDAD

We present additional qualitative results for KITTI in Fig. 13 and for DDAD in Fig. 11 and Fig. 12.

### 6.3. Comparison to BoostingDepth

To adjust BoostingDepth to Packnet-SAN, we computed PackNet-SAN’s receptive field both theoretically and empirically and obtained a receptive field of 1028 pixels. We

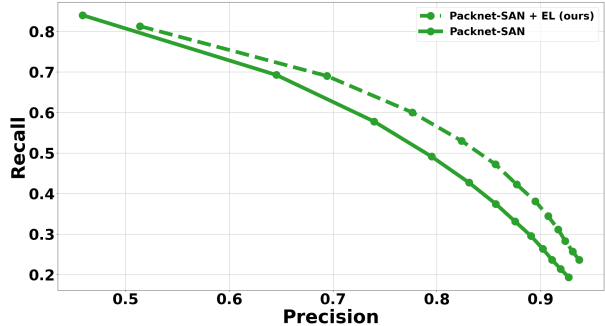


Figure 7. Precision and recall of the depth edges of the baseline vs. our method for Packnet-SAN on the Synscapes dataset.

utilize it as required by their method. For completeness, we also reported (in the main paper) the results of MIDAS [41] on our data, which was used as a baseline in BoostingDepth. The qualitative results are presented in Fig. 13.

## 6.4. Additional Details

### 6.4.1 The DEE Architecture

In Fig. 9 we present the architecture of the DEE network. This architecture is similar to the Packnet-SAN’s architecture, which is well suited for our purpose of processing both the dense RGB images and the sparse LIDAR signal.

### 6.4.2 The Input to The DEE network

As we argue in the main paper (L418), the performance of the DEE network is significantly better when the input is RGB and LIDAR, in contrast to RGB only. In Fig. 10 we present depth edges precision-recall graph for the DEE network, where the performance gap in favor of the RGB+LIDAR input is clearly present.

### 6.4.3 Depth Edge Loss

As we argue in the main paper (L370), using the standard spatial image gradient often yield undesired artifacts. See the stripes over the car silhouette for a depiction of this phenomenon in Fig. 8.

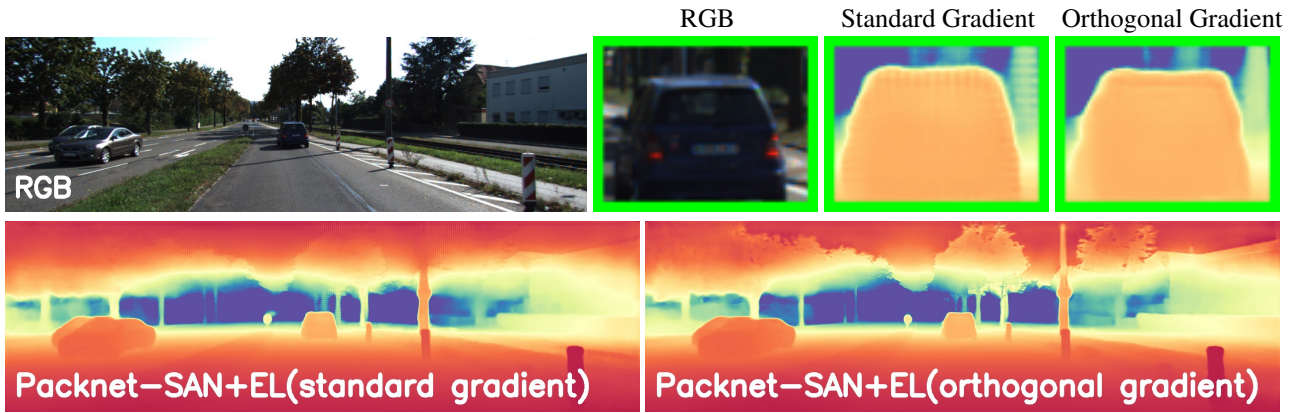


Figure 8. The standard spatial image gradient (named 'standard') and our proposed orthogonal to the edges spatial gradient (named 'orthogonal'). See Sec. 3.2 in the main paper for details.

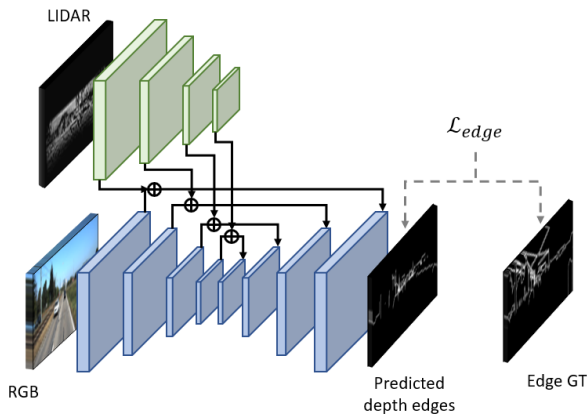


Figure 9. The architecture of the DEE model.

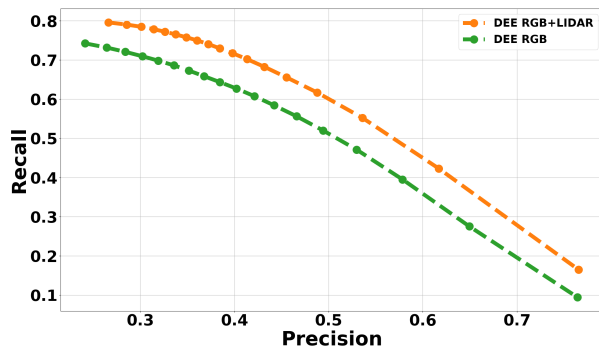


Figure 10. Precision and recall of the DEE model with RGB only and RGB+LIDAR inputs, inferred on the KITTI-DE dataset.

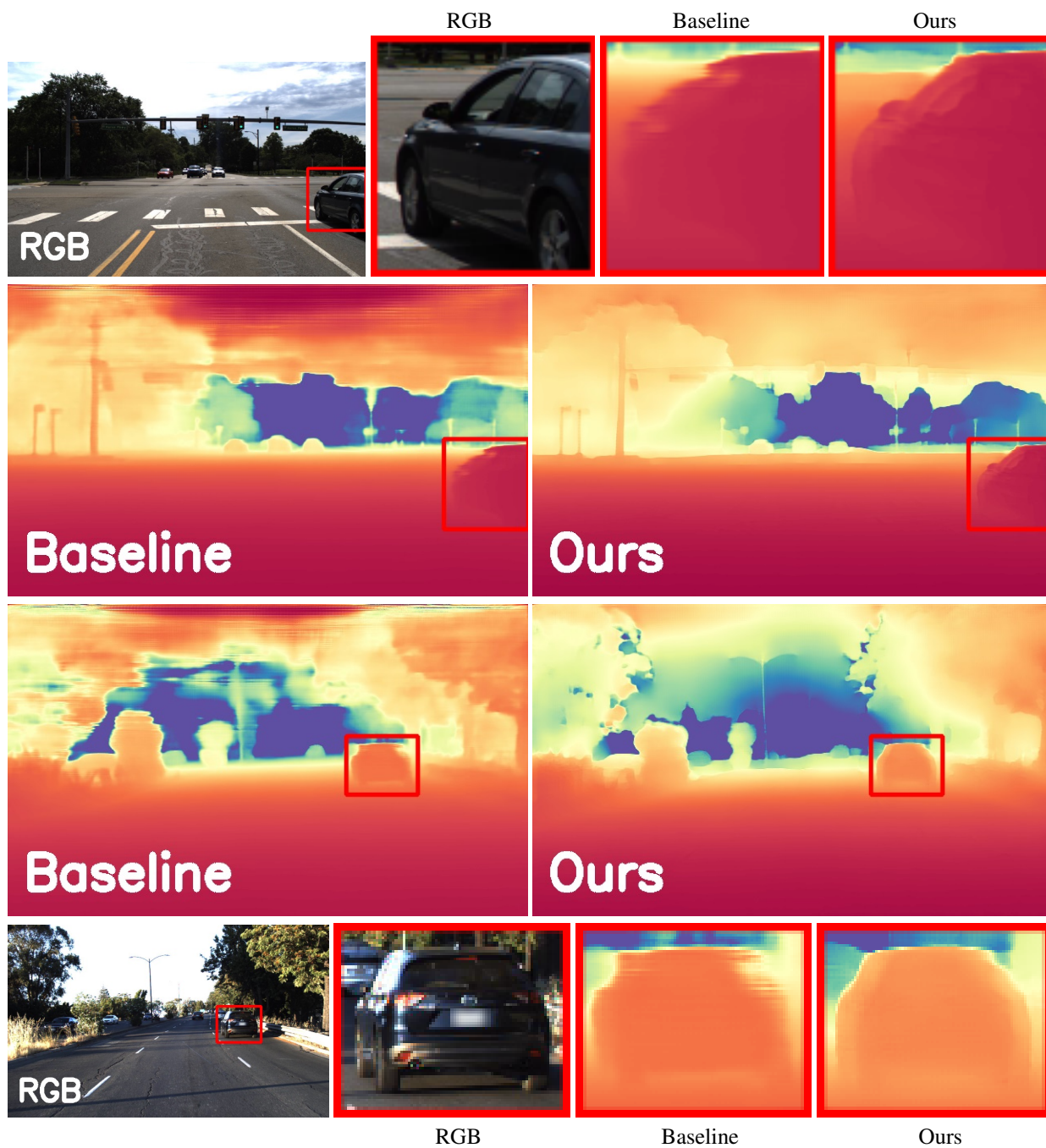


Figure 11. Examples of depth predictions of Packnet-SAN and Packnet-SAN + EL (ours) of images from the DDAD-DE dataset - Part I.

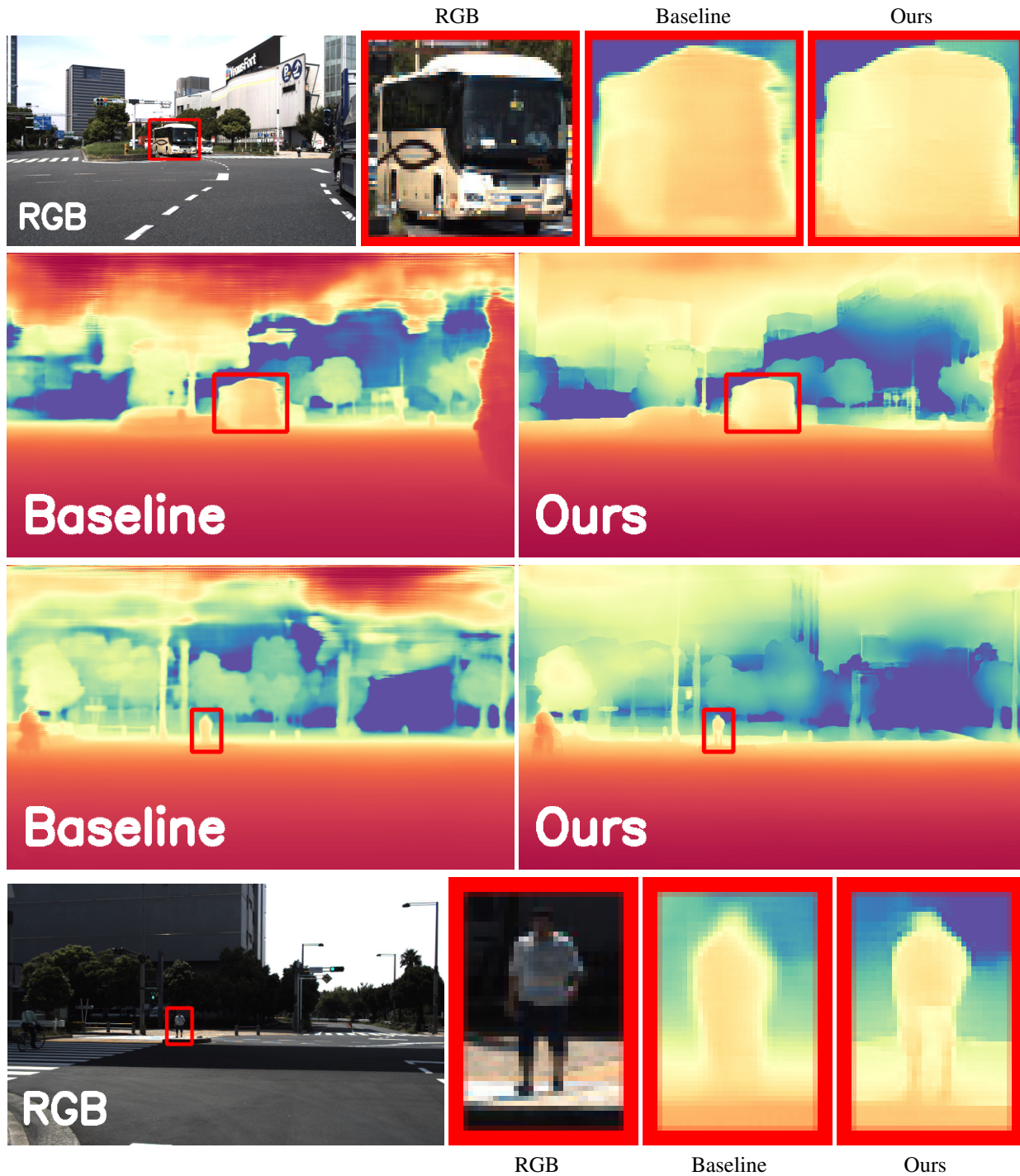


Figure 12. Examples of depth predictions of Packnet-SAN and Packnet-SAN + EL (ours) of images from the DDAD-DE dataset - Part II.

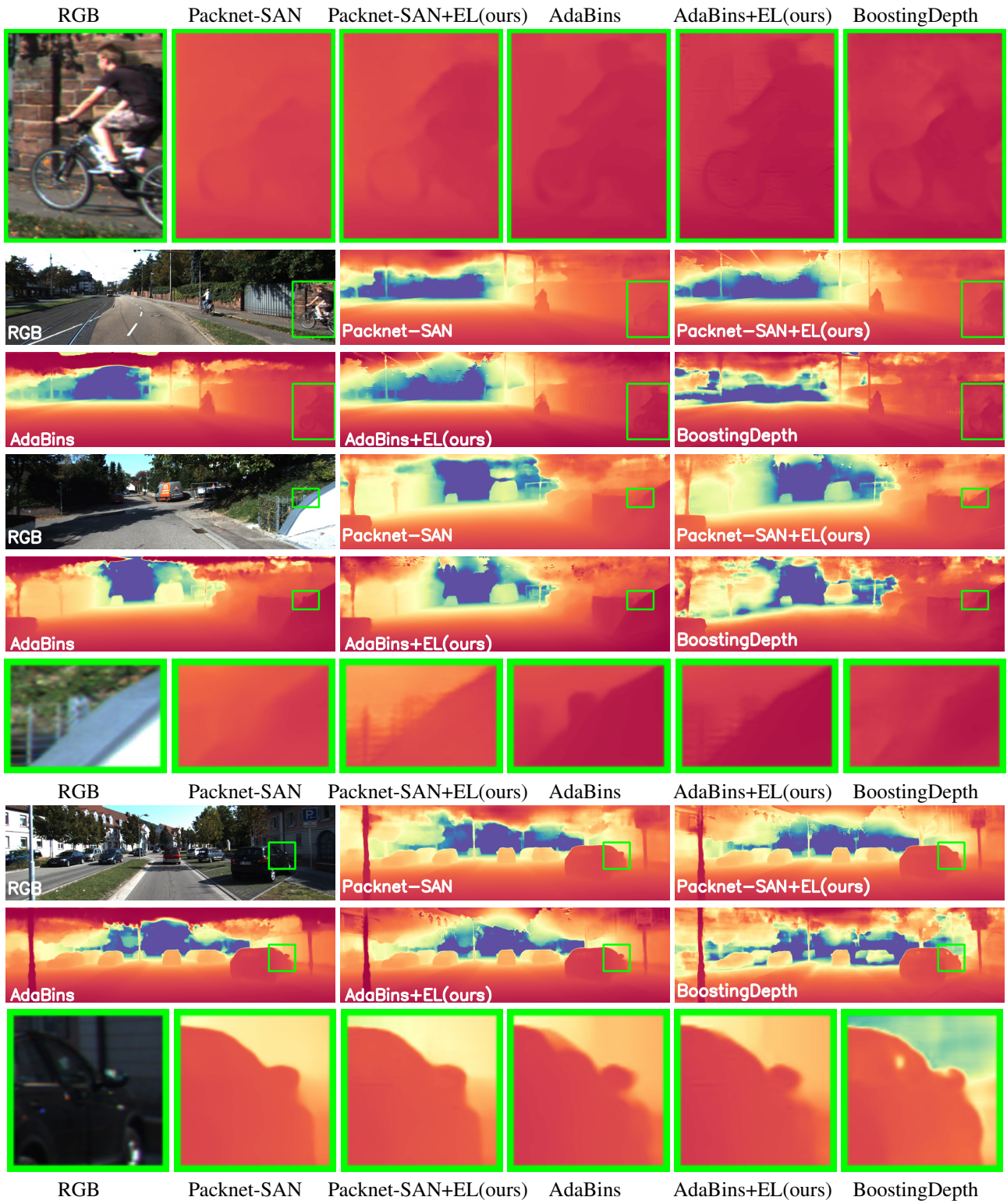


Figure 13. Examples of depth predictions of Packnet-SAN and Packnet-SAN + EL (ours) with and image from the KITTI-DE dataset.

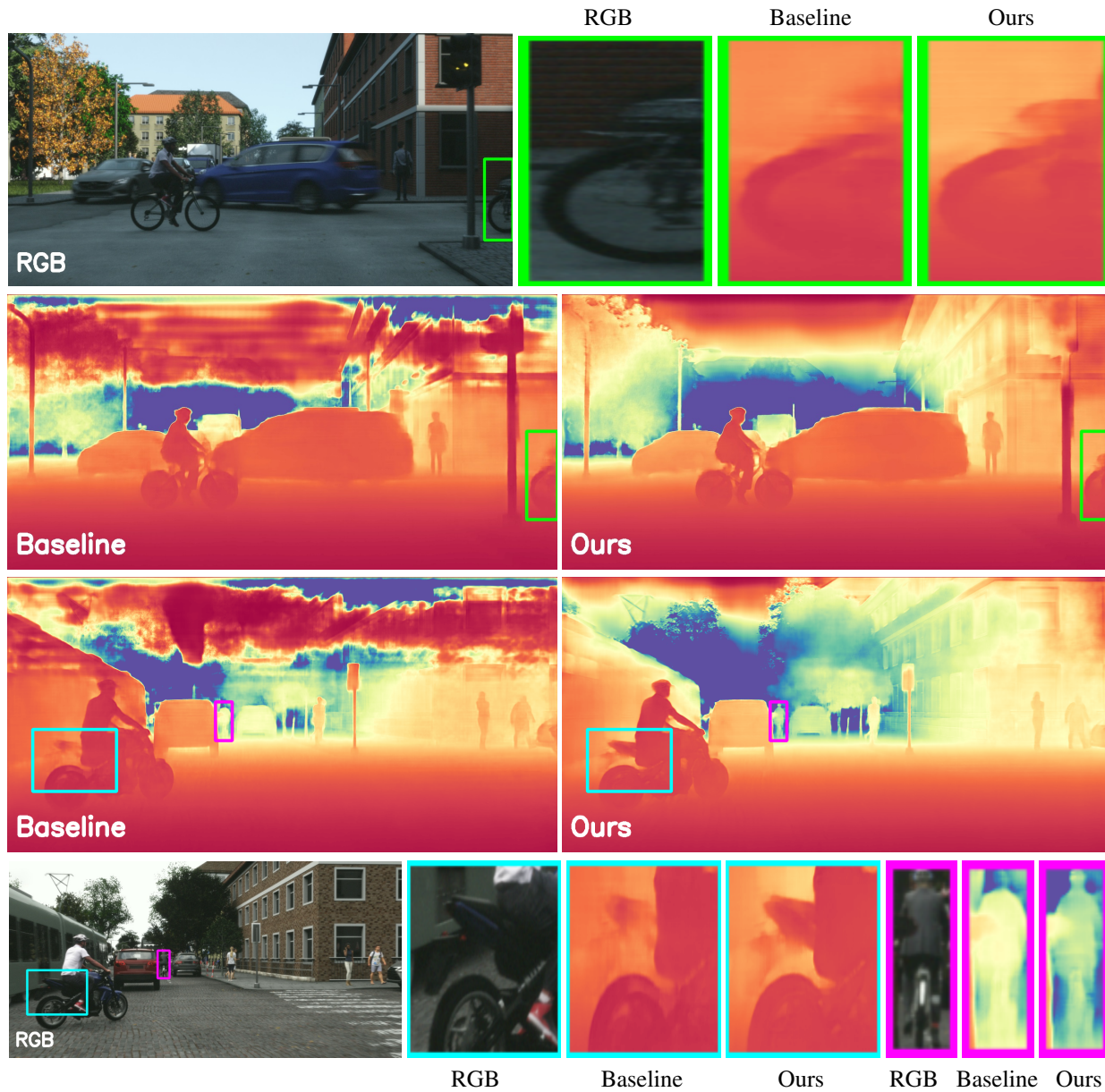


Figure 14. Examples of depth predictions of Packnet-SAN and Packnet-SAN + EL (ours) of images from the Synscapes dataset.

## References

- [1] Hassan Alhaija, Siva Mustikovela, Lars Mescheder, Andreas Geiger, and Carsten Rother. Augmented reality meets computer vision: Efficient data generation for urban driving scenes. *International Journal of Computer Vision (IJCV)*, 2018. 5
- [2] Ali Jahani Amiri, Shing Yan Loo, and Hong Zhang. Semi-supervised monocular depth estimation with left-right consistency using deep neural network. In *2019 IEEE International Conference on Robotics and Biomimetics (ROBIO)*, pages 602–607. IEEE, 2019. 3
- [3] Zuria Bauer, Zuoyue Li, Sergio Orts-Escolano, Miguel Cazorla, Marc Pollefeys, and Martin R Oswald. Nvs-monodepth: Improving monocular depth prediction with novel view synthesis. In *2021 International Conference on 3D Vision (3DV)*, pages 848–858. IEEE, 2021. 3
- [4] Shariq Farooq Bhat, Ibraheem Alhashim, and Peter Wonka. Adabins: Depth estimation using adaptive bins. In *Proceedings of the IEEE/CVF Conference on Computer Vision and Pattern Recognition*, pages 4009–4018, 2021. 3, 6
- [5] Yohann Cabon, Naila Murray, and Martin Humenberger. Virtual kitti 2. *arXiv preprint arXiv:2001.10773*, 2020. 3
- [6] John Canny. A computational approach to edge detection. *IEEE Transactions on pattern analysis and machine intelligence*, (6):679–698, 1986. 4, 5
- [7] Ang Cao, Chris Rockwell, and Justin Johnson. Fwd: Real-time novel view synthesis with forward warping and depth. In *Proceedings of the IEEE/CVF Conference on Computer Vision and Pattern Recognition*, pages 15713–15724, 2022. 1, 2
- [8] Vincent Casser, Soeren Pirk, Reza Mahjourian, and Anelia Angelova. Depth prediction without the sensors: Leveraging structure for unsupervised learning from monocular videos. In *Proceedings of the AAAI conference on artificial intelligence*, volume 33, pages 8001–8008, 2019.
- [9] Xiaotian Chen, Yuwang Wang, Xuejin Chen, and Wenjun Zeng. S2r-depthnet: Learning a generalizable depth-specific structural representation. In *Proceedings of the IEEE/CVF Conference on Computer Vision and Pattern Recognition*, pages 3034–3043, 2021. 3
- [10] Xuelian Cheng, Yiran Zhong, Yuchao Dai, Pan Ji, and Hongdong Li. Noise-aware unsupervised deep lidar-stereo fusion. In *Proceedings of the IEEE/CVF Conference on Computer Vision and Pattern Recognition*, pages 6339–6348, 2019. 2
- [11] Diogo Santos Ortiz Correa, Diego Fernando Sciotti, Marcos Gomes Prado, Daniel Oliva Sales, Denis Fernando Wolf, and Fernando Santos Osório. Mobile robots navigation in indoor environments using kinect sensor. In *2012 Second Brazilian Conference on Critical Embedded Systems*, pages 36–41. IEEE, 2012. 1
- [12] David Eigen, Christian Puhrsch, and Rob Fergus. Depth map prediction from a single image using a multi-scale deep network. *Advances in neural information processing systems*, 27, 2014. 5
- [13] Adrien Gaidon, Qiao Wang, Yohann Cabon, and Eleonora Vig. Virtual worlds as proxy for multi-object tracking analysis. In *Proceedings of the IEEE conference on computer vision and pattern recognition*, pages 4340–4349, 2016. 3, 5
- [14] Ravi Garg, Vijay Kumar Bg, Gustavo Carneiro, and Ian Reid. Unsupervised cnn for single view depth estimation: Geometry to the rescue. In *European conference on computer vision*, pages 740–756. Springer, 2016. 5
- [15] Andreas Geiger, Philip Lenz, and Raquel Urtasun. Are we ready for autonomous driving? the kitti vision benchmark suite. In *2012 IEEE conference on computer vision and pattern recognition*, pages 3354–3361. IEEE, 2012. 1, 2
- [16] Clément Godard, Oisín Mac Aodha, Michael Firman, and Gabriel J Brostow. Digging into self-supervised monocular depth estimation. In *Proceedings of the IEEE/CVF International Conference on Computer Vision*, pages 3828–3838, 2019. 3
- [17] Ariel Gordon, Hanhan Li, Rico Jonschkowski, and Anelia Angelova. Depth from videos in the wild: Unsupervised monocular depth learning from unknown cameras. In *Proceedings of the IEEE/CVF International Conference on Computer Vision*, pages 8977–8986, 2019. 3
- [18] Vitor Guizilini, Rares Ambrus, Wolfram Burgard, and Adrien Gaidon. Sparse auxiliary networks for unified monocular depth prediction and completion. In *Proceedings of the IEEE/CVF Conference on Computer Vision and Pattern Recognition*, pages 11078–11088, 2021. 1, 3, 5, 6
- [19] Vitor Guizilini, Rares Ambrus, Sudeep Pillai, Allan Raventos, and Adrien Gaidon. 3d packing for self-supervised monocular depth estimation. In *Proceedings of the IEEE/CVF Conference on Computer Vision and Pattern Recognition*, pages 2485–2494, 2020. 3
- [20] Vitor Guizilini, Rares Ambrus, Sudeep Pillai, Allan Raventos, and Adrien Gaidon. 3d packing for self-supervised monocular depth estimation. In *IEEE Conference on Computer Vision and Pattern Recognition (CVPR)*, 2020. 5
- [21] Vitor Guizilini, Rares Ambrus, Dian Chen, Sergey Zakharov, and Adrien Gaidon. Multi-frame self-supervised depth with transformers. In *Proceedings of the IEEE/CVF Conference on Computer Vision and Pattern Recognition*, pages 160–170, 2022. 3
- [22] Vitor Guizilini, Kuan-Hui Lee, Rares Ambrus, and Adrien Gaidon. Learning optical flow, depth, and scene flow without real-world labels. *IEEE Robotics and Automation Letters*, 7(2):3491–3498, 2022. 3
- [23] Vitor Guizilini, Igor Vasiljevic, Rares Ambrus, Greg Shakhnarovich, and Adrien Gaidon. Full surround monodepth from multiple cameras. *IEEE Robotics and Automation Letters*, 7(2):5397–5404, 2022. 3
- [24] Akhil Gurrām, Ahmet Faruk Tuna, Fengyi Shen, Onay Urfalioglu, and Antonio M López. Monocular depth estimation through virtual-world supervision and real-world sfm self-supervision. *IEEE Transactions on Intelligent Transportation Systems*, 2021. 3
- [25] Braden Hurl, Krzysztof Czarnecki, and Steven Waslander. Precise synthetic image and lidar (presil) dataset for autonomous vehicle perception. In *2019 IEEE Intelligent Vehicles Symposium (IV)*, pages 2522–2529. IEEE, 2019. 2, 5

- [26] Lam Huynh, Phong Nguyen-Ha, Jiri Matas, Esa Rahtu, and Janne Heikkilä. Guiding monocular depth estimation using depth-attention volume. In *European Conference on Computer Vision*, pages 581–597. Springer, 2020. 3
- [27] Phillip Isola, Jun-Yan Zhu, Tinghui Zhou, and Alexei A Efros. Image-to-image translation with conditional adversarial networks. In *Proceedings of the IEEE conference on computer vision and pattern recognition*, pages 1125–1134, 2017. 8
- [28] Alex Kendall, Hayk Martirosyan, Saumitro Dasgupta, Peter Henry, Ryan Kennedy, Abraham Bachrach, and Adam Bry. End-to-end learning of geometry and context for deep stereo regression. In *Proceedings of the IEEE international conference on computer vision*, pages 66–75, 2017. 3
- [29] Tobias Koch, Lukas Liebel, Friedrich Fraundorfer, and Marco Korner. Evaluation of cnn-based single-image depth estimation methods. In *Proceedings of the European Conference on Computer Vision (ECCV) Workshops*, pages 0–0, 2018. 3
- [30] Yevhen Kuznietsov, Jorg Stuckler, and Bastian Leibe. Semi-supervised deep learning for monocular depth map prediction. In *Proceedings of the IEEE conference on computer vision and pattern recognition*, pages 6647–6655, 2017. 3
- [31] Jin Han Lee, Myung-Kyu Han, Dong Wook Ko, and Il Hong Suh. From big to small: Multi-scale local planar guidance for monocular depth estimation. *arXiv preprint arXiv:1907.10326*, 2019. 3
- [32] Zhengqi Li and Noah Snavely. Megadepth: Learning single-view depth prediction from internet photos. In *Proceedings of the IEEE conference on computer vision and pattern recognition*, pages 2041–2050, 2018. 3
- [33] Marcio C de F Macedo and Antonio L Apolinario. Occlusion handling in augmented reality: Past, present and future. *IEEE Transactions on Visualization and Computer Graphics*, 2021. 1, 2
- [34] David R Martin, Charless C Fowlkes, and Jitendra Malik. Learning to detect natural image boundaries using local brightness, color, and texture cues. *IEEE transactions on pattern analysis and machine intelligence*, 26(5):530–549, 2004. 6
- [35] S Mahdi H Miangoleh, Sebastian Dille, Long Mai, Sylvain Paris, and Yagiz Aksoy. Boosting monocular depth estimation models to high-resolution via content-adaptive multi-resolution merging. In *Proceedings of the IEEE/CVF Conference on Computer Vision and Pattern Recognition*, pages 9685–9694, 2021. 1, 3, 7, 8
- [36] Andra Petrovai and Sergiu Nedevschi. Exploiting pseudo labels in a self-supervised learning framework for improved monocular depth estimation. In *Proceedings of the IEEE/CVF Conference on Computer Vision and Pattern Recognition*, pages 1578–1588, 2022. 3
- [37] Koutilya PNVR, Hao Zhou, and David Jacobs. Sharingan: Combining synthetic and real data for unsupervised geometry estimation. In *Proceedings of the IEEE/CVF Conference on Computer Vision and Pattern Recognition*, pages 13974–13983, 2020. 2
- [38] Michael Ramamonjisoa, Yuming Du, and Vincent Lepetit. Predicting sharp and accurate occlusion boundaries in monocular depth estimation using displacement fields. In *Proceedings of the IEEE/CVF Conference on Computer Vision and Pattern Recognition*, pages 14648–14657, 2020. 3
- [39] Michael Ramamonjisoa and Vincent Lepetit. Sharpnet: Fast and accurate recovery of occluding contours in monocular depth estimation. In *Proceedings of the IEEE/CVF International Conference on Computer Vision Workshops*, pages 0–0, 2019. 3
- [40] René Ranftl, Alexey Bochkovskiy, and Vladlen Koltun. Vision transformers for dense prediction. In *Proceedings of the IEEE/CVF International Conference on Computer Vision*, pages 12179–12188, 2021. 3
- [41] René Ranftl, Katrin Lasinger, David Hafner, Konrad Schindler, and Vladlen Koltun. Towards robust monocular depth estimation: Mixing datasets for zero-shot cross-dataset transfer. *IEEE transactions on pattern analysis and machine intelligence*, 2020. 3, 9
- [42] Faraz Saeedan and Stefan Roth. Boosting monocular depth with panoptic segmentation maps. In *Proceedings of the IEEE/CVF Winter Conference on Applications of Computer Vision*, pages 3853–3862, 2021. 3
- [43] Swami Sankaranarayanan, Yogesh Balaji, Arpit Jain, Ser Nam Lim, and Rama Chellappa. Learning from synthetic data: Addressing domain shift for semantic segmentation. In *Proceedings of the IEEE conference on computer vision and pattern recognition*, pages 3752–3761, 2018. 2
- [44] Daniel Scharstein, Heiko Hirschmüller, York Kitajima, Greg Krathwohl, Nera Nešić, Xi Wang, and Porter Westling. High-resolution stereo datasets with subpixel-accurate ground truth. In *German conference on pattern recognition*, pages 31–42. Springer, 2014. 3
- [45] Thomas Schops, Johannes L Schonberger, Silvano Galliani, Torsten Sattler, Konrad Schindler, Marc Pollefeys, and Andreas Geiger. A multi-view stereo benchmark with high-resolution images and multi-camera videos. In *Proceedings of the IEEE Conference on Computer Vision and Pattern Recognition*, pages 3260–3269, 2017. 3
- [46] Chang Shu, Kun Yu, Zhixiang Duan, and Kuiyuan Yang. Feature-metric loss for self-supervised learning of depth and egomotion. In *European Conference on Computer Vision*, pages 572–588. Springer, 2020. 3
- [47] Nathan Silberman, Derek Hoiem, Pushmeet Kohli, and Rob Fergus. Indoor segmentation and support inference from rgb-d images. In *European conference on computer vision*, pages 746–760. Springer, 2012. 1, 3
- [48] Minsoo Song, Seokjae Lim, and Wonjun Kim. Monocular depth estimation using laplacian pyramid-based depth residuals. *IEEE transactions on circuits and systems for video technology*, 31(11):4381–4393, 2021. 3
- [49] Kunal Swami, Amrit Muduli, Uttam Gurrām, and Pankaj Bajpai. Do what you can, with what you have: Scale-aware and high quality monocular depth estimation without real world labels. In *Proceedings of the IEEE/CVF Conference on Computer Vision and Pattern Recognition*, pages 988–997, 2022. 3
- [50] Zachary Teed and Jia Deng. Deepv2d: Video to depth with differentiable structure from motion. *arXiv preprint arXiv:1812.04605*, 2018. 3

- [51] Jonas Uhrig, Nick Schneider, Lukas Schneider, Uwe Franke, Thomas Brox, and Andreas Geiger. Sparsity invariant cnns. In *International Conference on 3D Vision (3DV)*, 2017. 5
- [52] Benjamin Ummenhofer, Huizhong Zhou, Jonas Uhrig, Nikolaus Mayer, Eddy Ilg, Alexey Dosovitskiy, and Thomas Brox. Demon: Depth and motion network for learning monocular stereo. In *Proceedings of the IEEE conference on computer vision and pattern recognition*, pages 5038–5047, 2017. 3
- [53] Igor Vasiljevic, Nick Kolkin, Shanyi Zhang, Ruotian Luo, Haochen Wang, Falcon Z Dai, Andrea F Daniele, Mohammadreza Mostajabi, Steven Basart, Matthew R Walter, et al. Diode: A dense indoor and outdoor depth dataset. *arXiv preprint arXiv:1908.00463*, 2019. 3
- [54] Yufeng Wang, Yi-Hsuan Tsai, Wei-Chih Hung, Wenrui Ding, Shuo Liu, and Ming-Hsuan Yang. Semi-supervised multi-task learning for semantics and depth. In *Proceedings of the IEEE/CVF Winter Conference on Applications of Computer Vision*, pages 2505–2514, 2022. 5
- [55] Jamie Watson, Oisin Mac Aodha, Victor Prisacariu, Gabriel Brostow, and Michael Firman. The temporal opportunist: Self-supervised multi-frame monocular depth. In *Proceedings of the IEEE/CVF Conference on Computer Vision and Pattern Recognition*, pages 1164–1174, 2021. 3
- [56] Felix Wimbauer, Nan Yang, Lukas Von Stumberg, Niclas Zeller, and Daniel Cremers. Monorec: Semi-supervised dense reconstruction in dynamic environments from a single moving camera. In *Proceedings of the IEEE/CVF Conference on Computer Vision and Pattern Recognition*, pages 6112–6122, 2021. 3
- [57] Magnus Wrenninge and Jonas Unger. Synscapes: A photorealistic synthetic dataset for street scene parsing. *arXiv preprint arXiv:1810.08705*, 2018. 5
- [58] Ke Xian, Jianming Zhang, Oliver Wang, Long Mai, Zhe Lin, and Zhiguo Cao. Structure-guided ranking loss for single image depth prediction. In *Proceedings of the IEEE/CVF Conference on Computer Vision and Pattern Recognition*, pages 611–620, 2020. 1, 3, 5
- [59] Saining Xie and Zhuowen Tu. Holistically-nested edge detection. In *Proceedings of the IEEE international conference on computer vision*, pages 1395–1403, 2015. 4
- [60] Yan Xu, Xinge Zhu, Jianping Shi, Guofeng Zhang, Hujun Bao, and Hongsheng Li. Depth completion from sparse lidar data with depth-normal constraints. In *Proceedings of the IEEE/CVF International Conference on Computer Vision*, pages 2811–2820, 2019. 2
- [61] Shanshan Zhao, Huan Fu, Mingming Gong, and Dacheng Tao. Geometry-aware symmetric domain adaptation for monocular depth estimation. In *Proceedings of the IEEE/CVF Conference on Computer Vision and Pattern Recognition*, pages 9788–9798, 2019. 3
- [62] Yunhan Zhao, Shu Kong, Daeyun Shin, and Charless Fowlkes. Domain decluttering: Simplifying images to mitigate synthetic-real domain shift and improve depth estimation. In *Proceedings of the IEEE/CVF Conference on Computer Vision and Pattern Recognition*, pages 3330–3340, 2020. 3
- [63] Zixiang Zhao, Jianshe Zhang, Shuang Xu, Zudi Lin, and Hanspeter Pfister. Discrete cosine transform network for guided depth map super-resolution. In *Proceedings of the IEEE/CVF Conference on Computer Vision and Pattern Recognition*, pages 5697–5707, 2022. 3
- [64] Tinghui Zhou, Matthew Brown, Noah Snavely, and David G Lowe. Unsupervised learning of depth and ego-motion from video. In *Proceedings of the IEEE conference on computer vision and pattern recognition*, pages 1851–1858, 2017. 3
- [65] Shengjie Zhu, Garrick Brazil, and Xiaoming Liu. The edge of depth: Explicit constraints between segmentation and depth. In *Proceedings of the IEEE/CVF Conference on Computer Vision and Pattern Recognition*, pages 13116–13125, 2020. 1, 3